Planetary and Space Science 145 (2017) 28–37

Contents lists available at ScienceDirect

Planetary and Space Science

journal homepage: www.elsevier.com/locate/pss

Response of the Martian ionosphere to solar activity including SEPs and ICMEs in a two-week period starting on 25 February 2015

F. Duru [a,d,*], D.A. Gurnett [a], D.D. Morgan [a], J. Halekas [a], R.A. Frahm [b], R. Lundin [c], W. Dejong [d], C. Ertl [d], A. Venable [d], C. Wilkinson [d], M. Fraenz [e], F. Nemec [f], J.E.P. Connerney [g], J.R. Espley [g], D. Larson [h], J.D. Winningham [b], J. Plaut [i], P.R. Mahaffy [g]

[a] Dept. of Physics and Astronomy, University of Iowa, Iowa City, IA 52242, USA
[b] Southwest Research Inst., PO Drawer 28510, San Antonio, TX 28228, USA
[c] Swedish Institute of Space Physics, Box 812, SE-981 28, Kiruna, Sweden
[d] Dept. of Physics, Coe College, Cedar Rapids, IA 52402, USA
[e] Max Planck Institute for Solar System Research, 37077 Gottingen, Germany
[f] Faculty of Mathematics and Physics, Charles University in Prague, Czech Republic
[g] NASA/Goddard Space Flight Center, Greenbelt, MD 20771, USA
[h] University of California at Berkeley, Berkeley, CA, USA
[i] Jet Propulsion Laboratory, M/S 183-601, 4800 Oak Grove Drive, Pasadena, CA 91109, USA

A B S T R A C T

In a two-week period between February and March of 2015, a series of interplanetary coronal mass ejections (ICMEs) and solar energetic particle (SEP) events encountered Mars. The interactions were observed by several spacecraft, including Mars Express (MEX), Mars Atmosphere and Volatile Evolution Mission (MAVEN), and Mars Odyssey (MO). The ICME disturbances were characterized by an increase in ion speed, plasma temperature, magnetic field magnitude, and energetic electron flux. Furthermore, increased solar wind density and speeds, as well as unusually high local electron densities and high flow velocities were detected on the nightside at high altitudes during the March 8 event. These effects are thought to be due to the transport of ionospheric plasma away from Mars. In the deep nightside, the peak ionospheric electron density at the periapsis of MEX shows a substantial increase, reaching number densities about 2.7×10^4 cm^{-3} during the second ICME in the deep nightside. This corresponds to an increase in the MO High-Energy Neutron Detector flux suggesting an increase in the ionization of the neutral atmosphere due to the high intensity of charged particles. Measurements of the SEP fluxs show a substantial enhancement before the shock of a fourth ICME causing impact ionization and absorption of the surface echo intensity which drops to the noise levels, below 10^{-15} V^{2}m^{-2} Hz^{-1} from values of about 2×10^{-14} V^{2}m^{-2} Hz^{-1}. Moreover, the peak ionospheric density exhibits a discrete enhancement over a period of about 30 h around the same location, which may be due to impact ionization. Ion escape rates at this time are estimated to be in the order of 10^{25} to 10^{26} s^{-1}.

1. Introduction

Studying space weather events provides important insight into the escape processes and the evolution of the planetary atmospheres. Coronal mass ejections (CMEs) are massive bursts of plasma and magnetic field originating from the Sun's corona (see Howard et al., 2014). They are termed ICMEs as they propagate through the interplanetary medium. ICMEs are observed to propagate radially away from the Sun at speeds greater than the typical solar wind velocity and are often preceded by a shock wave. Emission across a wide range of photon and particle energies is associated with strong CMEs and strong flares. It is known that the ion escape processes are enhanced when ICMEs interact with the atmospheres and ionospheres of unmagnetized planets (Futaana et al., 2008; Dubinin et al., 2009; Edberg et al., 2010).

The discovery and description of ICMEs have a long and complex history (see, e.g. the historical summary by Howard, 2014). The characteristics of ICMEs are usually described in terms of probabilities because all of the characteristics of an ICME are rarely observed at the same time and for the same event. The root cause of a CME is the sudden release of magnetic energy bound up in the solar corona. After initiation in the corona, the CME develops into a rapidly moving mass of solar particles. Propagation speeds are usually 300–1000 km/s but can be higher, with the total mass of the ejected material typically 10^{11}–10^{12} kg (see Howard, 2014). This mass of particles moves at speeds significantly greater than the ambient solar wind and can develop a detectable shock front (see Forbes et al., 2006). The ICME catalog described by Chi et al.

* Corresponding author. University of Iowa, Dept. of Physics and Astronomy, Iowa City, IA 52242, USA.
E-mail address: firdevs-duru@uiowa.edu (F. Duru).

http://dx.doi.org/10.1016/j.pss.2017.07.010
Received 28 November 2016; Received in revised form 17 July 2017; Accepted 20 July 2017
Available online 22 July 2017
0032-0633/

(2016) shows virtually all ICMEs with velocity greater than 400 km/s developing a shock at Earth orbit. After the shock there is often a region of disturbed plasma, called the sheath, followed by a traveling flux rope also known as a magnetic cloud (see Howard, 2014). The magnetic cloud can be rarefied compared to the surrounding plasma. We say "often" because the flux rope characteristic is not always observed; furthermore, it is not clear whether they are not observed because of observational issues or because the characteristics of the flux ropes are not there in all cases. Forbes et al. (2006) stated that a lack of clearly observed flux rope morphology could be due to an innate difference between types of ICMEs, spacecraft trajectory through the body of an ICME, or complexity due to collisions among several magnetic structures. According to Chi et al. (2016), about one-third of observed ICMEs contain a structure meeting several criteria for a magnetic cloud, or traveling flux rope. Where there is a shock, ions are accelerated to solar energetic particle (SEP) energies (~1 MeV). Gopalswamy et al. (2002) make a strong case that ICMEs produce SEPs primarily when a slow ICME is overtaken by a faster one. The effect at a given planet is determined by the solar wind magnetic field connection between the interaction region and the planetary atmosphere. The specific effects of the intense magnetic fields and energetic particles at Mars are described by many studies including Opgenoorth et al. (2013) and Morgan et al. (2014). These effects include energization of ionospheric electrons, intrusion of solar wind electrons into the ionosphere, compression and possible erosion of the ionosphere, and strong impulsive intensification of the magnetic field. Because solar flares sometimes occur in approximate coincidence with a CME at the Sun, impulsive SEP events can be associated with ICMEs, whereas shock-driven SEPs are observed as so-called gradual events (Forbes et al., 2006). It is known that SEP events are related to ICMEs (Reames, 1999). When an ICME occurs the charged particles from the solar wind start to move along the magnetic field lines. Since SEPs move much faster than the ICME shock they arrive earlier than the shock if the magnetic field lines are connected to the planet.

There have been several studies of the influence of space weather events on the environment of Mars. For example, Crider et al. (2005) concluded that there was a strong compression of the Martian ionosphere during the Halloween Superstorm of 2003. Espley et al. (2005) and Futaana et al. (2008) investigated solar flare events in October 2003 and December 2006. Opgenoorth et al. (2013) studied the effect of three space weather events on Mars concluding, again, that significant ionospheric compression and heavy ion energization occurs when ICMEs interact with the Mars ionosphere. Past studies have also shown that SEP events cause enhanced electron density in the ionosphere, which is seen from attenuation of the surface reflection during space weather events with MARSIS radar data (see, e.g. Morgan et al., (2006), Nemec et al., (2014)). There has been some simulation efforts, as well, such as McKenna-Lawlor et al. (2008), who made predictions of the interplanetary shocks during December 2006 solar flares. The effects of solar weather on the ion escape fluxes are modeled by Ma and Nagy (2007). More recently, the effects of a strong ICME at Mars were studied by Morgan et al. (2014) using Mars Express (MEX) and Mars Odyssey (MO) observations. All these studies had to rely on extrapolations of the upstream solar wind conditions since no upstream solar wind monitor was available. Finally, Jakosky et al. (2015) showed the response of Mars to the ICME on March 8, 2015, using data which provided information about the upstream solar wind from Mars Atmosphere and Volatile Evolution Mission (MAVEN) solar wind monitors. Data from the MAVEN Solar Wind Ion Analyzer (SWIA) (Halekas et al., 2015) and the Magnetometer (MAG) (Connerney et al., 2015a,b) were used to generate the escape rates in the regions affected by the ICMEs. Their observations will be used for comparison purposes in this study.

In a two-week period between February 25, 2015 and March 13, 2015, a series of ICMEs were detected by multiple spacecraft studying the ionosphere and solar wind environment of Mars. At least four ICMEs were observed during this period, the last of which, on March 8, was very strong. Using the data from six instruments on three different spacecraft, we first investigate the two-week period as a whole, then we study the effects of the ICME events on the solar wind environment and ionosphere of Mars focusing on the final March 8 event.

In the period starting on February 25, 2015 and ending on March 13, 2015, which has been studied extensively by MAVEN (Jakosky et al., 2015), the orbit of MEX spacecraft had its periapsis in the deep nightside of Mars allowing examination of the effects of an ICME in this region. During the same period, the MAVEN spacecraft scanned solar zenith angles (SZA) between about 38° and 142°, being on the dayside when the fourth and strongest event's shock is observed. Finally, MO spacecraft periodically covered a region between about 63° and 117° SZA. This high level of coverage makes it possible to perform a comprehensive investigation of this series of ICME interactions, comparing the effects observed in different regions of Mars. In this paper our objective is to present results from the Mars Express radar sounder that complement the MAVEN an MO observations and add to the understanding of this complicated event and its interaction with Mars.

2. Instruments

Data from six instruments on three spacecraft, MEX, MAVEN, and MO, are studied in order to understand the effect of the ICMEs, which occurred from February 25 to March 13, day 56 to day 72, of 2015.

MEX has been in an orbit around Mars since December 25, 2005, with six instruments monitoring changes in the Martian environment. One of these instruments is the Mars Advanced Radar for Subsurface and Ionospheric Sounding (MARSIS) instrument, which is a low-frequency radar. MARSIS, which consists of a 40 m tip-to-tip dipole antenna, a 7 m monopole antenna, a radio transmitter, a receiver and a digital processing system (Picardi et al., 2004), provides ionospheric density profiles determined by using a remote radar sounding technique (Gurnett et al., 2005). When an ionospheric profile is visible, the peak ionospheric density can be identified. MARSIS is also able to obtain the local plasma density and the local magnetic field strength from measurements of local electron plasma frequency harmonics and electron cyclotron echoes on ionograms, which are plots of echo intensity as a function of time delay and frequency (Gurnett et al., 2005; Duru et al., 2008; Akalin et al., 2010). To perform remote sounding, a short radio pulse with frequency f is emitted and the time delay to the returning echo is measured. This process is repeated every 7.54 s for 160 quasi-logarithmic steps at frequencies between 100 kHz and 5.5 MHz. Waves that are incident normal to the reflective surface of the ionosphere are reflected back to the sounder. For normal incidence, the reflection occurs at the altitude where the frequency of the wave transmitted by the sounder is equal to the electron plasma frequency.

An example ionogram is shown in Fig. 1, which is taken from Duru et al. (2010). This plot shows the echo intensity as a function of time delay on the vertical axis, and frequency on the horizontal axis. At lower frequencies, between 1.0 and 1.85 MHz in this ionogram from November 11, 2007, an ionospheric echo is observed. The highest frequency in the ionospheric echo, denoted by f_p (max) in the figure, is the peak electron density in the ionosphere. Surface reflections are only detected at frequencies greater than f_p (max).

The vertical, equally spaced lines in the upper left corner of Fig. 1 are harmonics of electron plasma oscillations, which are due to instrumental distortion of electron plasma oscillations excited locally by the sounder (Duru et al., 2008). The spacing between two consecutive lines provides the electron plasma frequency local to the spacecraft, f_p, which in turn can be used to calculate the local electron density using $n_e = (f_p)^2/(8\ 980)^2$, where f_p is in Hz and n_e is the local electron density in cm^{-3}.

The equally spaced horizontal lines on the left side of the ionogram are electron cyclotron echoes. The time difference between these horizontal lines is used to calculate the magnitude of the local magnetic field (Gurnett et al., 2010; Akalin et al., 2010).

The MEX Analyzer of Space Plasmas and Energetic Atoms (ASPERA-

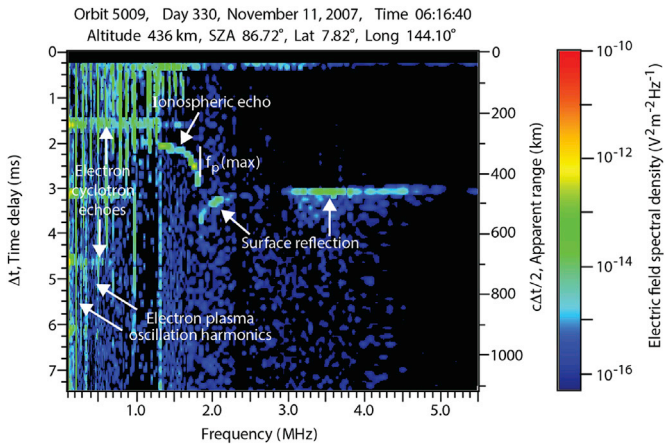

Fig. 1. Sample ionogram from November 11, 2007 (from Duru et al. (2010), Fig. 1b). The received intensity is indicated by the plotted color according to the color bar. The electron plasma oscillations, electron cyclotron echoes, ionospheric echo, surface reflection, and peak density in the ionosphere (f_p (max)) are shown. (For interpretation of the references to colour in this figure legend, the reader is referred to the web version of this article.)

3) instrument is a suite of plasma and neutral detectors that consists of an electron spectrometer (ELS), an ion mass analyzer (IMA), a neutral particle detector (NPD), a neutral particle imager (NPI), and a digital processing unit (Barabash et al., 2004, 2006). ELS is an electron spherical top-hat analyzer with a 360° × 4° field of view divided into 16 angular sectors that provides measurements in 127 logarithmic stepsfrom about 1 eV to 20 keV every 4 s (Barabash et al., 2006; Frahm et al., 2006). IMA is an ion top-hat energy analyzer coupled with an elevation analyzer at its entrance and a magnetic momentum analyzer at its exit. The IMA field of view is 360° × ±45°, divided into 16 steps of elevation and 16 azimuthal sectors. IMA measures ion distributions from ~-25 eV/q to 20 keV/q in 96 energy steps, and mass per charge spectra up to about 40 amu/q (Barabash et al., 2006). The ion fluxes for different energies can be used to derive ion flow velocities, including the solar wind speed.

MAVEN, which arrived at Mars in September 2014, studies the solar wind interactions of the upper atmosphere, and investigates atmospheric evolution and escape processes (Jakosky et al., 2015). MAVEN carries of three science packages. Its particle and fields package consists of a Solar Wind Electron Analyzer (SWEA) (Mitchell et al., 2016), a Solar Wind Ion Analyzer (SWIA) (Halekas et al., 2013), a Solar Energetic Particle instrument (***SEP***) (Larson et al., 2015), Suprathermal and Thermal Ion Composition instrument (STATIC) (McFadden et al., 2015), a Langmuir Probe (LPW) (Andersson et al., 2015) with the Extreme Ultraviolet (EUV) Monitor (Eparvier et al., 2015), and a Magnetometer (MAG) (Connerney et al., 2015a; 2015b). MAVEN's Imaging Ultraviolet Spectrometer (IUVS) is a remote sounding package and its Neutral Gas and Ion Mass Spectrometer (NGIMS) package is the mass spectrometry instrument. In this paper, we present data from SWIA, which provides ion flow measurements in the magnetosheath, the upstream solar wind and the magnetotail. SWIA provides proxy solar wind and neutral density measurements, in addition to directly measured solar wind protons and alpha particles upsteam Mars (Halekas et al., 2017). The toroidal energy analyzer and elevation analyzer on SWIA provides a field of view of 360° × 90° on a 3-axis stabilized spacecraft. MAG, which consists of two independent, tri-axial fluxgate magnetometer sensors, measures the magnetic field in the solar wind and ionosphere of Mars (Connerney et al., 2015a). Some of the issues about MAG, such as compensating for spacecraft magnetic fields and verifying the accuracy of the measurements for weak fields are explained in Connerney et al. (2015b). *SEP* (here we use the italic font for the MAVEN instrument to distinguish it from the particles from Sun SEP) measures energetic electrons (between 25 keV and 1 MeV) and protons (between 25 keV and 6 MeV) with 4 telescopes using dual-side solid state crystal technology (Larson et al., 2015).

Finally, the High-Energy Neutron Detector (HEND) is part of the Gamma Ray Spectrometer suite of instruments onboard the MO spacecraft. Its main purpose is to study energetic neutrons (Boynton et al., 2004), however, it has a special channel designed to detect X-rays and charged particles. We use this channel as a solar energetic particle detector.

3. Data

The data from MEX and MAVEN during the disturbed period from day 56 (Feb. 25) of 2015 to day 72 (March 13) of 2015 are presented in Fig. 2 as a time series in six stacked plots. Panel (a) displays the solar wind speed obtained from spectral fits to the ion mass analyzer data on ASPERA-3, which is able to provide the solar wind speed when the solar wind H^+ kinetic energy is above 1 keV or when there is a clean He^{++} signal. The speed is almost constant at about 400 km/s near the beginning of the period. Towards the end of day 57, starting from 22:15 UT, a small increase is observed. The solar wind speed gradually goes back to about 400 km/s until about 18:16 UT on day 62 where it abruptly increases by about 50%. It stays almost constant up to about day 68, except for a small peak on day 66. Around 15:20 UT on day 67 (March 8), the solar wind speed suddenly increases to 1000 km/s, from which it rapidly decreases. Each rise in the solar wind speed, marked by a dashed line, is an indication of a shock associated with the ICMEs. The solar wind speeds obtained by SWIA display similar behavior for this period (Jakosky et al., 2015).

Panel b of Fig. 2 shows the solar wind density obtained with SWIA on MAVEN. The ICME impacts on the ionosphere are associated with increases in the solar wind plasma density. At the start of the interval, the spacecraft is in the undisturbed solar wind, where the plasma density is ~5 cm^{-3}. Near the first solar wind velocity increase detected by ASPERA-3 IMA, the plasma density reaches ~25 cm^{-3}. Near the second such increase, the peak is ~20 cm^{-3}. Between day 66 and 71, which includes the third and fourth events, the density has four distinct peaks with values changing between 8 cm^{-3} and 4 cm^{-3}. The larger of these peaks is nearly coincident with the solar wind velocity increases detected by ASPERA-3 IMA shown in Panel (a).

The magnetic field magnitude from MAG is shown in Panel (c), which also exhibits peaks closely following the dashed lines. In order to make sure that the spacecraft is measuring the solar wind magnetic field, we used the bow shock model from Vignes et al. (2000), obtained using the Mars Global Surveyor (MGS) observations to filter out data not taken when MAVEN is in the solar wind. For every orbit a series of the magnetic field vectors are obtained and the smallest vector magnitude has been chosen to be displayed. All four ICME shock times correspond to a peak in the magnitude of the magnetic field. During the final event, a smaller peak is followed by a more substantial one reaching values of 16 nT.

In Panel (d) the solar energetic ion spectra for high energy ions, collected by the ***SEP*** instrument onboard MAVEN, are shown. For each ICME an enhancement in the ion flux is observed closely following each of the solar wind velocity increases. Note that the intensification in the highest energy ion flux is observed about a day before the shock of the strongest ICME, which is an expected behavior (Jakosky et al., 2015). Part of this enhancement can also be due to previous events. Also note, that the third solar wind velocity increase, which is very small, is associated with a very small enhancement in the energetic ion flux.

Panel (e) displays electron spectra for different energies from ASPERA-3 ELS. Again, the increase in the flux by about an order of magnitude can be observed at the times of the events.

Finally, the local electron density from MARSIS Active Ionospheric Sounding (AIS) is presented in Panel (f). Data are shown for altitudes above 1 200 km in order to exclude the high densities in the ionosphere at low altitudes. Since there are multiple values for each orbit, the local electron densities for a given pass look like a vertical line on the time scale shown in Fig. 2. Even with the lower limit on the altitude, high local electron densities are observed around the times of the ICMEs, especially

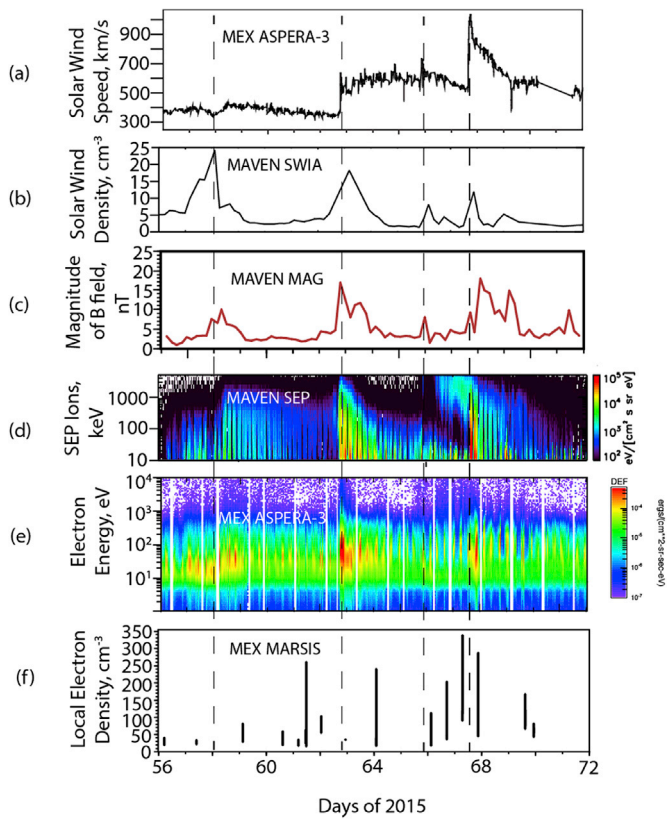

Fig. 2. Time series of several measured quantities during the two-week period from Feb. 25 to March 13, 2015. The observations indicate that four ICMEs impacted at Mars, marked by the dashed lines. Panel (a): Solar wind speed from ASPERA-3 IMA. Panel (b): Solar wind density from SWIA. Panel (c): Magnitude of magnetic field in the solar wind from MAG. Panel (d): High energy ion flux from *SEP*. Panel (e): Electron flux from ASPERA-3 ELS. Panel (f): Local electron density above 1 200 km from MARSIS. (Panels (b) and (d) are taken from Jakosky et al., (2015).).

before the last event, which we believe is due to SEPs' encounter with the Martian upper ionosphere. Also, during the last event, the magnetic field magnitude obtained with MARSIS through electron cyclotron echoes (not shown) reaches 40 nT, which is about 4 times the usual value, and it is about 55 nT on day 63 (March 4) which corresponds to the second event.

The enhancement of SEPs, which penetrate deep into the ionosphere has been shown to cause absorption of the ground reflection (see e.g. Morgan et al., (2006), Nemec et al., (2014)). The top panel of Fig. 3 presents the surface echo intensity during the two-week period in question (for more information on how surface reflection is calculated see Nemec et al. (2015)). The intensities are obtained from MARSIS remote sounding using altitudes between 350 and 450 km and SZA higher than 107°. The median intensity is taken for each orbit. The horizontal dashed line at about 4.5×10^{-14} $V^2/m^2/Hz$ is the normally expected surface echo intensity without absorption. There is a large depletion between the start and end of the period, with two possible partial recoveries in between. The middle and bottom panels show the SEP electrons and ions, respectively. The enhancements in the SEP ions and electrons are in excellent agreement with the surface intensity reductions. The drops in the intensity, especially at the times of intense high energy electron fluxes, are in accordance with the fact that the high-energy electrons penetrate deeper in the atmosphere than lower-energy electrons, causing additional ionization.

The behavior of the peak density in the ionosphere, obtained remotely by the MARSIS sounder, and the HEND charged particle/X-ray intensities are shown in Fig. 4. Panel (a) of this figure is the same as the top panel of Fig. 2. It displays the solar wind speed obtained from ASPERA-3 for comparison purposes. The peak density at the periapsis from MARSIS remote ionospheric sounding is shown in the middle panel and indicates fluctuations. However, since the spacecraft is on the nightside, the density is always below 1.5×10^4 cm^{-3} except for one time at the end of day 62. At this time, which corresponds to the shock of the second ICME, the peak electron density becomes more than twice the highest peak density recorded during this time interval, reaching 2.7×10^4 cm^{-3}. This increase occurs at the same time as the depletion in the surface intensity and enhancements in the SEP electrons and ions.

The bottom panel (c) displays the count rate of charged particles and X-rays from the HEND instrument, with energies from hundreds of keV up to several MeV. The count rate is just below 4×10^3 s^{-1} for most of the period, and has a small peak for the second ICME, which corresponds to the big peak in the peak electron density. This substantial increase in the peak ionospheric density can be explained by the increased charged particle fluxes in the solar wind, which increase the ionization. A strong peak is observed between days 65 and 67, the period in which the third ICME occurred and had the weakest effect on other instruments, impacted the ionosphere of Mars. However, this time range corresponds to the enhanced SEP electrons (see Fig. 3).

A closer look at the MARSIS local electron density is provided in Figs. 5 and 6. Each figure shows five orbits and the dashed line indicates the periapsis location on each of the passes, which is drawn to mark the center of each orbit. The local electron density as a function of time of a selection of orbits between days 60 and 62 is displayed in Fig. 5. Orbits which are featureless and have a small amount of data are not displayed. In addition, plots are not displayed for orbits where the ionospheric sounder was not operating. Though the electron density is highly variable (see Gurnett et al., (2010)), in all five of these orbits the density shows an increasing trend as the spacecraft descends (except maybe for orbit 14, 171 which has a very irregular trend). According to a MARSIS survey of the local electron densities on the nightside of Mars by Duru et al. (2011), the electron density values at the location of the spacecraft are generally very low, changing between 2 500 cm^{-3} (around the terminator region, in the altitude range between 200 and 400 km) and 40 cm^{-3} (in the SZA range between 130 and 140° and altitude range between 1 200 and 1 400 km). The electron density values shown in this figure are within the error bars of the study mentioned above. The shock of the second ICME occurs directly right after the pass of orbit 14,173. During the next two available orbits, the electron density is almost constant at ~100 cm^{-3}.

Fig. 6 shows that the local electron densities at high altitudes around the time of the fourth ICME (the shock is seen at the end of March 8, day 67) are much higher than predicted. For the first orbit in the figure, the electron densities in the altitude range between 400 and 800 km reach values of ~500 cm^{-3}, which is above the average for that range. The

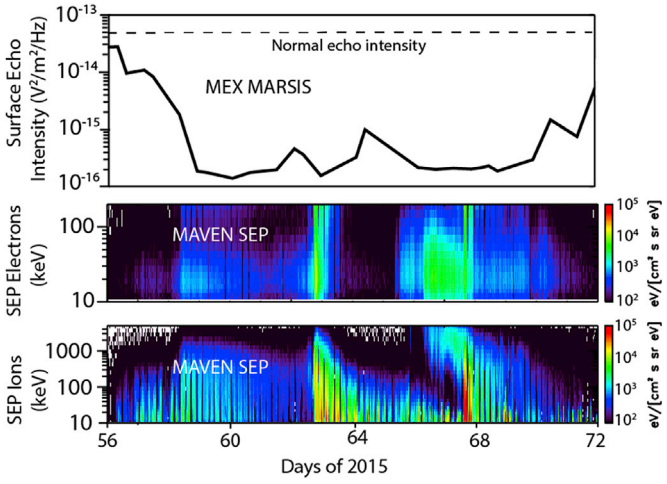

Fig. 3. Top panel: The surface echo intensity in the altitude range between 350 and 450 km and SZA > 107° during the two-week period in question. The dashed-line indicates expected surface echo intensity when there is no absorption. Middle panel: High energy electron flux from *SEP*. Bottom panel: High energy ion flux from *SEP*.

electron densities reach very high values on passes from orbits 14,186 and 14,188. The densities above 700 km reach values above 800 cm^{-3}, which is more than 5 times the average values noted in Duru et al. (2011). Around this time the densities near periapsis, when available, are much lower than at higher altitudes.

To gain a more detailed understanding of the ICME interaction on the nightside, we focus on the last and strongest event which happened on March 8, 2015, and examine the ionograms from orbits around this time. They reveal that the electron plasma oscillation harmonics show unusually high spacing at the beginning of the pass, indicating that high local electron densities at very high altitudes are observed. As the spacecraft descends, the local electron plasma density decreases. When the plasma oscillations (observed as vertical lines in the ionograms) get very weak or disappear, a very diffused ionospheric echo is observed. This diffused reflection, indicating a turbulent ionosphere, is present for several minutes. After a few minutes the diffused reflection becomes distinct and sharp.

An intriguing feature is present in the plots of peak electron density obtained through MARSIS remote sounding (marked by A, B and C in Fig. 7). This "top-hat" feature, which is present in three orbits at the time of the ICME, is observed when the ionospheric echo on the ionograms becomes extended in frequency resulting in high peak density values. This feature is observed in all three cases in the first three panels of Fig. 6 and for all of these cases the crustal magnetic field is weak, with values less than 50 nT. The features do not correspond to the times of high local electron density (see the corresponding orbits in Fig. 6). All of these top-hat features are closer to periapsis than high local electron density regions. The only correspondence is between times 07:02 and 07:04 UT in orbit 14,188, where high peak electron densities and high local electron densities are observed at the same time. However, this time is 5 min before the top-hat shaped feature. Further investigation (the bottom panel of Fig. 7) shows this feature occurs at about the same SZA, local time (LT) and latitude for all three cases. The examination of the plots of echo intensity as a function of time and universal time at fixed frequency shows that the altitude of the peak electron density of the ionosphere is at about 160 km, which is the expected height of the ionosphere based on a Monte Carlo Model (Lillis et al., 2009). At the other times the height of the ionosphere is at about 140 km, which is about 20 km lower than

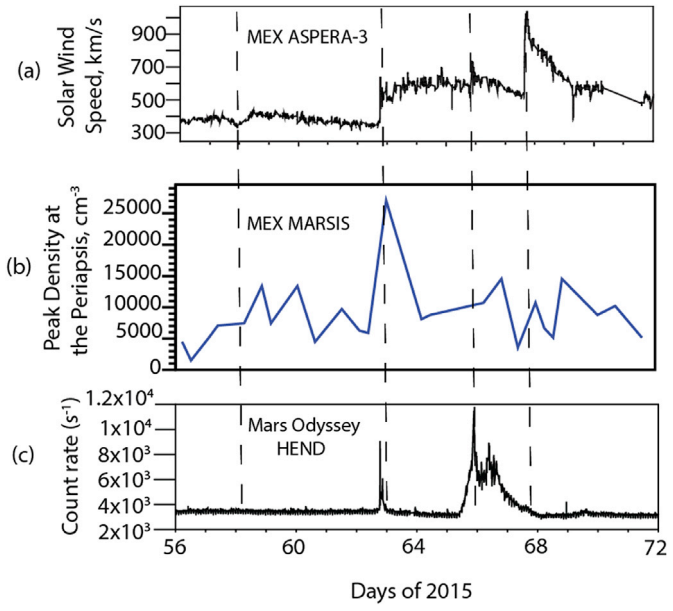

Fig. 4. The same two-week period as in Fig. 2, which displays 4 ICME events at Mars indicated by the dashed lines. Panel (a): Solar wind speeds obtained from ASPERA-3 IMA (kept for reference purposes). Panel (b): Peak electron density around periapsis from MARSIS remote sounding. Panel (c): Charged particle/X-ray count from HEND.

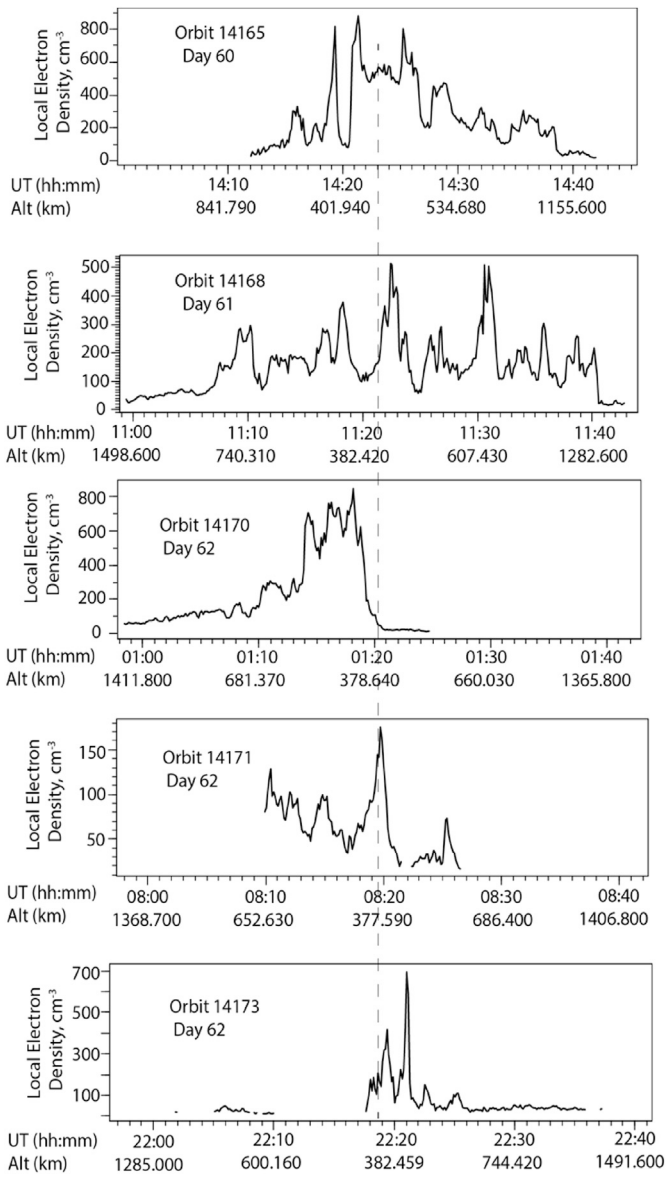

Fig. 5. The local electron plasma frequency as a function of universal time (UT) and altitude are shown for five passes on days 60, 61, and 62,. Periapsis is indicated by the dashed line.

usual. We believe this is due to the SEP precipitation. All three orbits occur during the final intensification of SEPs: More energetic particles will ionize the atmosphere at lower altitudes. In two of the cases, ASPERA-3 ELS detects electrons flowing away from the planet. This is consistent with the findings of a recent study by Withers et al. (2012), who state that peak altitudes of about 150 km are observed at SZA > 115° and much lower altitudes are detected during solar energetic particle events.

The "top-hat" features may indicate a cloud of plasma, which is being transported from the dayside plasma towards the nightside because of the strong solar wind, or these features may be a result of intense impact ionization due to very energetic particles. Post-terminator enhancements in the peak density have been seen in the past; however, a top-hat-like feature which lasts for several orbits is recorded for the first time.

4. Discussion and summary

In this study, presenta highly active and variable two-week period in the Martian ionosphere in 2015 is presented using measurements from

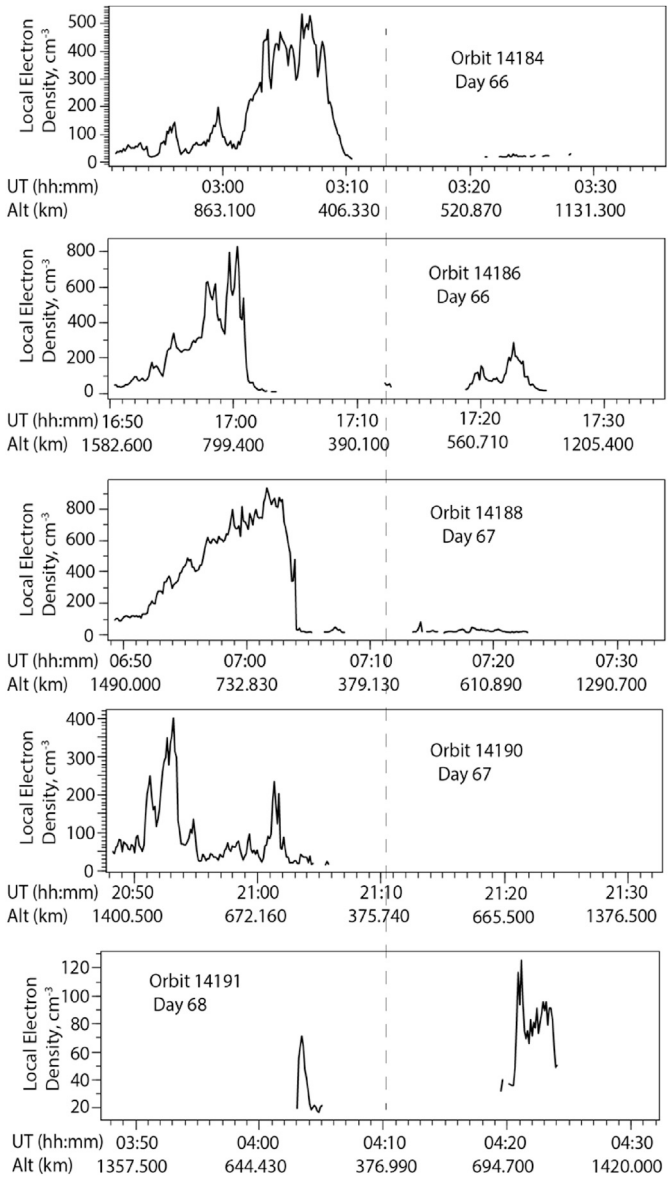

Fig. 6. The local electron plasma frequency as a function of universal time (UT) and altitude are shown for five passes: ondays 66),67) and68). Periapsis is indicated by the dashed line.

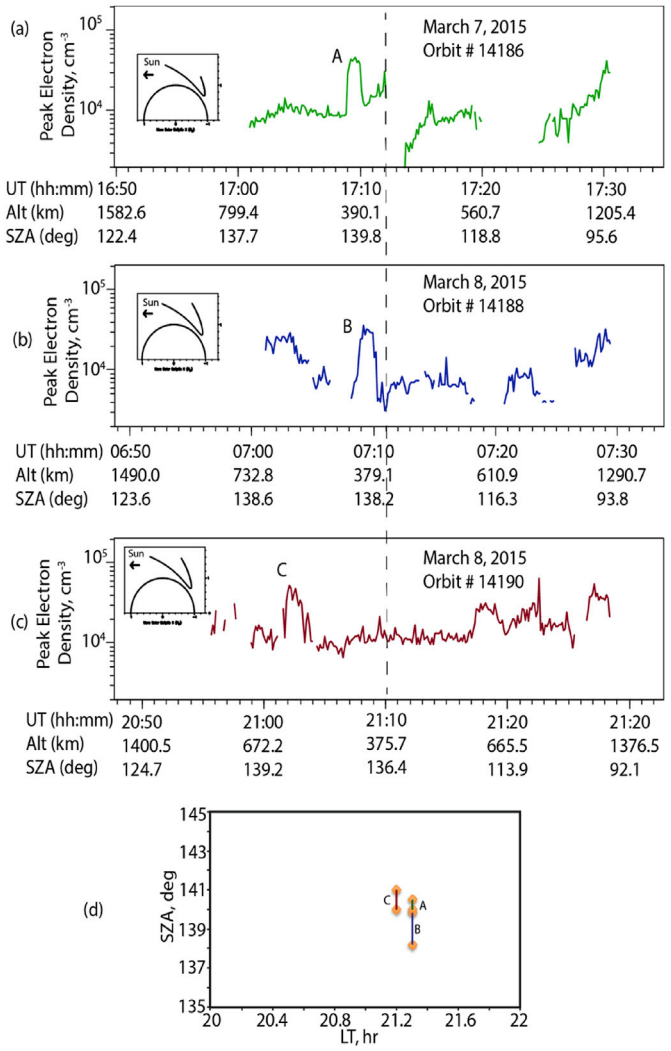

Fig. 7. Panel (a), (b) and (c) show peak electron density in the ionosphere from MARSIS remote sounding for orbits 14,186 (day 66), 14,888 (day 67) and 14,190 (day 67), respectively. Panel (d) presents the SZA and LT of the hat-shaped features present in three of the orbits. The beginning and end of the feature is marked and joined by a line for each pass.

three different spacecraft. At least four ICMEs are detected during this time frame and their effects are observed by all three spacecraft in different regions around the planet: MEX being in the deep nightside, and MAVEN and MO on the dayside. The strongest of these ICMEs occurred on March 8, 2015. Dong et al. (2015) provided a multifluid MHD study of the interaction between the solar wind and ionosphere of Mars. In addition to being the strongest ICME, it occurs during a more chaotic period of the ionosphere than during the previous ICMEs. The effects of the previous ICMEs caused turbulent ionospheric conditions which persisted when the March 8 ICME hit Mars. Also, the SEP electrons and ions are enhanced before the shock of this last ICME. Gopalswamy et al. (2002) concluded that the shock of a CME accelerates SEPs from the solar wind affected by preceding CMEs, instead of from the quiet solar wind. This statement is consistent with the appearance of SEPs before an ICME, which is preceded by three others in this two week period.

As expected, all the ICMEs are evident on examination of the solar wind speed obtained with ASPERA-3, which showed an increase in solar wind speed at each event indicating a shock. The solar wind speed increases are also consistent with peaks in the solar wind density and solar energetic particle flux determined by MAVEN.

There has been many studies showing that Mars has been losing part of its atmosphere. Lundin et al. (1989) reports about 3×10^{25} ions/s oxygen escape rate. A large fraction of the atmosphere loss is believed to be due the escape of plasma. Several studies have provided estimates of ion escape rates from the Martian ionosphere. Lundin et al. (1990) reports that the average total O+ ion escape in the tail is about 2×10^{25} ions/s according to ion composition experiment ASPERA on Phobos-2. According to Barabash et al. (2007), the highest rates are obtained for O^+ ions, reported to be 1.6×10^{23} s^{-1}. A more recent study provides evidence of solar cycle effects on the ion escape rates stating that the average heavy ion escape rate is about 1×10^{24} s^{-1} during solar minimum and 1×10^{25} s^{-1} during solar maximum (Lundin et al., 2013). Dong et al. (2017) states that the total ion escape rate for > 6 eV O^+ is 2.4×10^{24} s^{-1} and the total ion escape rate increases from 2.1 to 3.1×10^{24} s^{-1} as the EUV irradiance increases from 0.26 to 0.44 mW/m^2. These results are consistent with the calculations of Ma et al. (2014), where the modeled total ion escape rate is around 2.3×10^{24} s^{-1}.

Figs. 8 and 9, which will be used to make an estimate of the escape rate, provide data for two orbits on March 8, 2015, where the highest local electron densities are obtained. The bottom panels (Panels (d)) show the local electron densities determined from MARSIS. The flow

velocities for O^+ (blue) and O_2^+ (green) ions calculated with ASPERA-3 data are given in Panels (c). Expected local electron density values for the given altitude and solar zenith angle range determined using MARSIS are indicated by the red horizontal lines, which are the average values taken from Duru et al. (2011). The purple line marks the location of the top-hat feature for the given orbit. During the ICME, the local electron densities reach very high values, about eight times the expected density in some cases. The ion flow velocities are around 10–20 km/s for the high density regions. Panels (a) and (b) show the total heavy ion flux and heavy ion outflow obtained from IMA, respectively.

The heavy ion flux and corresponding heavy ion outflow from IMA shown on Panels (a) and (b) is provided as a lower limit to the escape rate. The ion flux from IMA changes in the range between 2×10^5 and 2×10^7 $cm^{-2}s^{-1}$ on March 8. The ion outflow rate is about 8×10^{23} ions/s^{-1} at the beginning of pass 14,188. It increases after a drop. At around 7:13 UT on day 67 it reaches values as 1×10^{24}. At 20:50 UT (see Fig. 9), which is after the shock of the fourth ICME, the value is as high as 3×10^{24} ions/s. After this time, the outflow rate decreases to values around 10^{23} ions/s. However, it should be noted that the field of view of IMA is limited. Not only does IMA lack a 4 pi field of view, but at energies below 50 eV measurements are planar (the elevation analyzer voltage is set to zero for ions detected below 50 eV). The lack of angular coverage may lead to an overestimation of the velocities. Also, the lack of knowledge about the spacecraft potential can be misleading even though a potential correction is applied (Fraenz et al., 2015).

Jakosky et al. (2015) provided estimates of the ion escape rates using MAVEN data and a model during the March 8, 2015 ICME. We perform a simple estimate in order to compare with their results using these data, which requires some bold assumptions. Knowing the local electron density from electron plasma oscillations, and the ionospheric flow velocity from ASPERA-3 IMA, we can make a rough estimate of the ion escape rates during the ICME event. Since MEX is in the deep nightside, it also gives us an idea about how the ion escape rates change on the nightside with the solar wind interaction occurring on the dayside. In order to calculate the ion escape rates, we assume that the escape from the ionosphere of Mars is cylindrically symmetric. We are aware that it adds to the uncertainty, however, this is a necessity because of the available data we have. Considering a thin disk around the planet starting at the location of the data (see Fig. 10), the escape rate can be calculated by multiplying the average local density by the flow velocity and the area of the disk (given by $2\pi\rho\Delta\rho$, where ρ is the radius of the thin shell and $\Delta\rho$ is its thickness). Ion escape rates are calculated for the high density regions for the two passes shown in Figs. 8 and 9. For the first time period, which gives us the highest rates, the ion escape rate is found to be 9.1×10^{25} s^{-1} (using $\rho = 3\,371$ km, $\Delta\rho = 700$ km, and local $n_e = 600$ cm^{-3}) and for the second time period the ion escape rate is 3.2×10^{25} s^{-1} (using $\rho = 3\,371$ km, $\Delta\rho = 400$ km, and local $n_e = 200$ cm^{-3}). Both values are of the same order of magnitude as the results from Jakosky et al. (2015), who obtained ion escape rates of 1.46×10^{24} s^{-1}, 1.06×10^{25} s^{-1} and 3.34×10^{25} s^{-1} for three different stages of the ICME using MAVEN data and a model. The period for which we have determined the escape rates corresponds to the times just before and just after the ICME shock. Our first value, 9.1×10^{25} s^{-1}, obtained at about the same time Jakosky et al. (2015) computed the second value, 1.06×10^{25} s^{-1}, and our second value, 3.2×10^{25} s^{-1}, corresponds to the third case in Jakosky et al. (2015), 3.35×10^{25} s^{-1}. Our first value is somewhat higher, but of the same order of magnitude as the MAVEN results. However, it should be kept in mind that the technique used by Jakosky et al. (2015) does not take into account the influence of SEPs, which we believe is what increased the local electron density values even before the shock of the ICME. Our second time gives almost the exact same number for the escape rate. Another important point is the high uncertainty involved with our calculation. With a rough, but bold estimate, using $\Delta\rho_{error} = 200$ km, $\rho_{error} = 150$ km, $v_{error} = 2$ km/s we obtain an error of 1.7×10^{24} s^{-1}. Even with uncertainties in the higher end, the final error is an order of magnitude less than the actual values.

The values that we obtained are also about an order of magnitude higher than the numbers obtained by Lundin et al. (2013) for solar maximum times, which is expected during a strong ICME. According to Lundin et al. (2013), the heavy ion escape rates during solar minimum and maximum are 1×10^{24} and 1×10^{25} s^{-1}, respectively. During solar storm times it is expected to have one or two order of magnitude higher escape rates (Lundin et al., 2008; Nilsson et al., 2011; Ramstad et al., 2013). Even though the method used here is approximate, the results are reasonable when compared with the average ion escape rates, keeping in mind that the ion escape rates that were generated by the March 8 ICME are instantaneous values measured at a single point during a highly

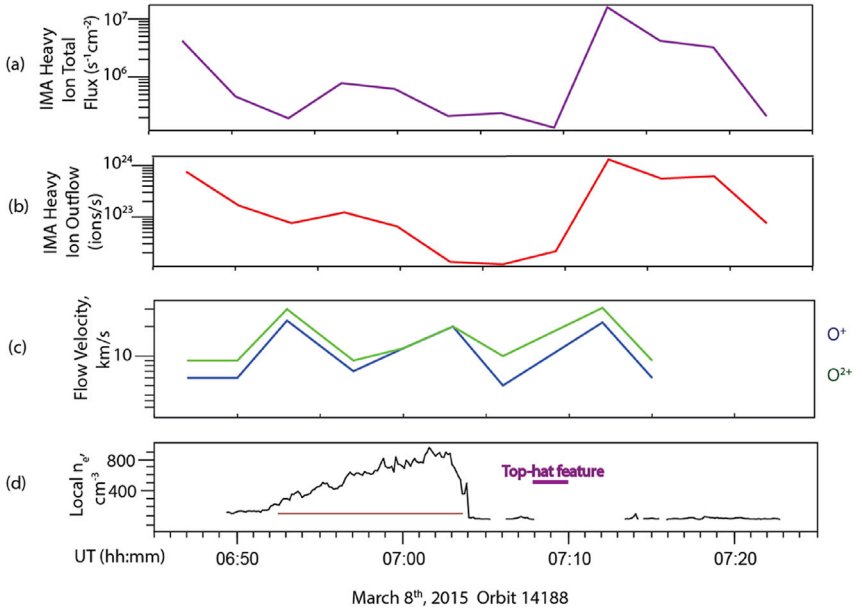

Fig. 8. Panel (a): Total heavy ion flux from ASPERA-3 IMA for the orbit 14,188 (day 67). Panel (b): Heavy ion outflow from IMA Panel (c): O+ (blue) and O2+ (green) flow velocities obtained from IMA. Panel (d): Corresponding local electron densities from MARSIS. The red line indicates the expected local electron density values in the given SZA and altitude range obtained from Duru et al. (2011). The thick purple lines on the local electron density plots indicate the location of the top-hat feature in these orbits. (For interpretation of the references to colour in this figure legend, the reader is referred to the web version of this article.)

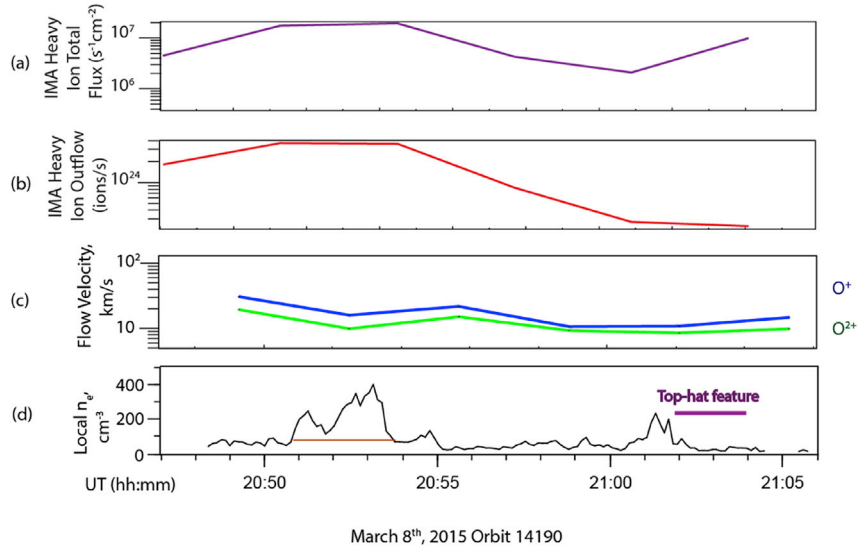

Fig. 9. In the same format as in Fig. 8, Panel (a): Total heavy ion flux from ASPERA-3 IMA for the orbit 14,190 (day 67). Panel (b): Heavy ion outflow from IMA Panel (c): O+ (blue) and O2+ (green) flow velocities obtained from IMA. Panel (d): Corresponding local electron densities from MARSIS. (For interpretation of the references to colour in this figure legend, the reader is referred to the web version of this article.)

dynamic period. The local electron densities at the given altitude and SZA range drop to the expected values (around 100 cm^{-3}). Since we do not have flow velocity data for the times outside the ICME, it is not possible to give exact numbers, but it is safe to assume that the escape rates should be about an order of magnitude less than during the ICME times. In addition to the errors in the measurements, the method used here provides an approximation of the escape rate determined by making use of several assumptions. The fact that the flux of particles is not actually cylindrically symmetric and that not all of the ions are above the escape velocity of Mars leaving the planet makes our results only an approximation. Similar methods have been previously used; however, they yield results in the same order of magnitude (10^{25} ions/s) for *trans*-terminator flow at Mars (Fraenz et al., 2010).

The charged particle/X-ray count rate from HEND shows a narrow peak right after the second ICME event, and a very wide peak between the third and fourth ICME events, where the count reached values around 1×10^4 s^{-1}. This behavior is consistent with the high energy ion and electron flux observed in the ***SEP*** instrument data. Peak electron density values around the periapsis for each available pass are studied at the times when HEND shows count peaks. The peak electron density obtained from MARSIS remote sounding reveals that there was a substantial increase at the time of the narrow peak in the HEND data, which is believed to be due to an increase in the ionization of the neutral atmosphere due to increased fluxes of X-rays and charged particles.

The SEP may originate from a new original flare, independent from the ICME, but they may be observed before the ICME if the ICME traveling from the Sun is magnetically connected to Mars. Jakosky et al. (2015) suggested that the SEP enhancements observed before the ICME on March 8, are due to the coming ICME. As SEP particles arrive at Mars, they will penetrate deep into the ionosphere causing ionization and possible absorption. The study of the surface reflection echo intensity shows that this is what is actually happening during this two weeks. The intensity is highly depleted during this time range, which drops from values about 4.5×10^{-14} $V^2/m^2/Hz$ to the noise level right around February 28 (day 59). Two possible recovery regions are observed peaking around days 62 and 65, which correspond to the low intensity regions on the *SEP* ions and electron plots. As the SEPs are enhanced the surface echo intensity is attenuated to noise level.

The local electron density from MARSIS for the altitudes above 1 200 km displays very high values exceeding 800 cm^{-3} around the time of the fourth ICME. High flow velocities at the same time suggest

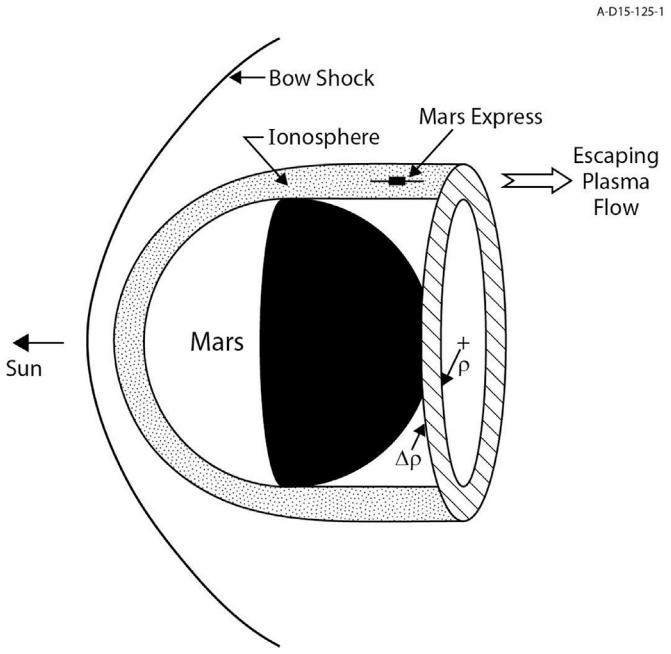

Fig. 10. The sketch of the ionosphere and solar wind environment of Mars. A thin disk is defined around Mars and used to calculate the escape rate of ions.

transport of plasma from the dayside to the nightside of Mars because of the pressure of the high speed and dense solar wind. The highest densities correspond to the times before the shock of the ICME where the SEPs are enhanced. Although, impact ionization due to high energy solar wind particles remains as another possible reason for very high electron densities, it is very unlikely since the altitudes are very high and the plasma is tenuous.

Investigation of three orbits around the last event shows that in general the altitude of the ionosphere is about 140 km, which is about 20 km less than the predicted value for the nightside. In this last ICME event, an exception to this idea is found in the observation of a persistent feature seen in the ionospheric peak electron density for three orbits at SZA between 138° and 141° and local time of 21.3 h. During these observations the altitude of the nightside ionosphere is about 160 km (the

top-hat feature presented in Fig. 6). No strong crustal fields are present in this region. This feature lasts about 2 min, which corresponds to a distance of about 500 km in the direction of the spacecraft, in each pass and is characterized by a hat-shaped appearance on the peak electron density plots. The features observed on orbits 14,186 and 14,188 are before the shock of the ICME. However, they happen at the time of the very strong signatures of SEP ions and electrons. During one of the three times investigated outward flowing electrons are observed by ELS. The ionospheric density peaks for the time of the top-hat featurecan be due to a localized and transient plasma cloud formed as a result of transport or impact ionization. Knowing that the SEPs (especially electrons) can penetrate deep in the ionosphere suggests that the density increase due to impact ionization is a likely scenario. SEP enhancements are decreased considerably after the shock of the ICME, which can be explained with the fact that shocks alter the magnetic field topologies.

This study provides a more complete look at the ionosphere of Marsof Mars in a time period with ICMEs and SEPs. Different instruments on three different space craft, which survey different parts of the Martian ionosphere, permits us to investigate the interaction between the solar wind and Mars from different angles. Since MEX is on the nightside during this time, it gives us an opportunity to study the effects of high solar activity after the terminator. The effect of the SEPs are very clear. We see that for the nightside density SEPs are a determining factor, whereas ICMEs affect the ion loss rates.

Acknowledgement

This paper describes observations obtained from both the NASA sponsored MAVEN and Mars Odyssey, and the ESA sponsored Mars Express mission to Mars. Data from Mars Express AIS and ASPERA-3 ELS and IMA are available from the NASA Planetary Data System (PDS) Geosciences Node (http://pds-geosciences.wustl.edu/). Data from Mars Odyssey Gamma Ray Spectrometer, High Energy Neutron Detector and MAVEN are also available from the NASA PDS Geosciences Node. We are grateful to these agencies for making this study possible. This work is funded by contract 156064 administered by the Jet Propulsion Laboratory at the University of Iowa, NASA contract NASW-00003 at Southwest Research Institute, and the Swedish National Space Board. Finally, we would like to thank Kathy Kurth for going over the text for us.

References

Akalin, F., Morgan, D.D., Gurnett, D.A., Kirchner, D.L., Brain, D.A., Modolo, R., Acuna, M.H., Espley, J.R., 2010. Dayside induced magnetic field in the ionosphere of Mars. ICARUS 206, 104–111. http://dx.doi.org/10.1016/j.icarus.2009.03.02.

Andersson, L., Weber, T.D., Malaspina, D., Crary, F., Ergun, R.E., Delory, G.T., Fowler, C.M., Morooka, M.W., McEnulty, T., Eriksson, A.I., Andrews, D.J., Horanyi, M., Collette, A., Yelle, R., Jakosky, B.M., 2015. Dust observations at orbital altitudes surrounding Mars. Science 350, aad0398.

Barabash, S., et al., 2004. ASPERA-3: analyser of space plasmas and energetic ions for Mars express. In: Wilson, A. (Ed.), Mars Express: a European Mission to the Red Planet. ESA Publications Division, ESTEC, Noordwijk, Netherlands, pp. 121–140.

Barabash, S., et al., 2006. The analyzer of space plasmas and energetic Atoms (ASPERA-3) for the Mars express mission. Space Sci. Rev. 126, 113–164. http://dx.doi.org/10.1007/s11214-006-9124-8.

Barabash, S., Fedorov, A., Lundin, R., Sauvaud, J.A., 2007. Martian atmospheric erosion rates. Science 315, 501–503. http://dx.doi.org/10.1126/science.1134358.

Boynton, W.V., et al., 2004. The Mars Odyssey gamma-ray spectrometer instrument suite. Space Sci. Rev. 110, 37–83.

Chi, Y., Shen, C., Wang, Y., Ye, P., Wang, S., 2016. Sol. Phys. 291, 8. http://dx.doi.org/10.1007/s11207-016-0971-5.

Connerney, J.E.P., Espley, J.R., Lawton, P., Murphy, S., Odom, J., Oliversen, R., Sheppard, D., 2015a. The MAVEN magnetic field investigation. Space Sci. Rev. http://dx.doi.org/10.1007/s11214-015-0169-4.

Connerney, J.E.P., Espley, J.R., DiBraccio, G.A., Gruesbeck, J.R., Oliversen, D.L., Mitchell, D.L., Halekas, J., Mazelle, C., Brain, D.A., Jakosky, B.M., 2015b. First results of the MAVEN magnetic field investigation. Geophys. Res. Lett. 42, 8819–8827. http://dx.doi.org/10.1002/2015GL065366.

Crider, D.H., Espley, J., Brain, D.A., Mitchell, D.L., Connerney, J.E.P., Acuna, M.H., 2005. Mars Global Surveyor observations of the Halloween 2003 solar superstorm's encounter with Mars. J. Geophys. Res. 110, A09S21. http://dx.doi.org/10.1029/2004JA010881.

Dong, C., Ma, Y., Bougher, S.W., Toth, G., Nagy, A.N., Halekas, J.S., Dong, Y., Curry, S.M., Luhmann, J.G., Brain, D., Connerney, J.E.P., Espley, J., Mahaffy, P., Benna, M., McFadden, J.P., Mitchell, D.L., DiBraccio, G.A., Lillis, R.J., Jakosky, B.M., Grebowsky, J.M., 2015. Multifluid MHD study of the solar wind interaction with Mars' upper atmosphere during the 2015 March 8th ICME event. Geophys. Res. Lett. 42 http://dx.doi.org/10.1002/2015GL065944.

Dong, Y., Fang, X., Brain, D.A., McFadden, J.P., Halekas, J.S., Connerney, J.E.P., Eparvier, F., Andersson, L., Mitchell, D., Jakosky, B.M., 2017. Seasonal variability of Martian ion escape through the plume and tail from MAVEN observations. J. Geophy. Res. Space Phys. 122, 4009–4022. http://dx.doi.org/10.1002/2016JA023517.

Dubinin, E., Fraenz, M., Woch, J., Duru, F., Gurnett, D., Modolo, R., Barabash, S., Lundin, R., 2009. Ionospheric storms on Mars: impact of the corotating interaction region. Geophys. Res. Lett. 36, L01105. http://dx.doi.org/10.1029/2008GL036559.

Duru, F., Gurnett, D.A., Morgan, D.D., Modolo, R., Nagy, A.F., Najib, D., 2008. Electron densities in the upper ionosphere of Mars from the excitation of electron plasma oscillations. J. Geophys. Res. 113, A07302. http://dx.doi.org/10.1029/2008JA013073.

Duru, F., Morgan, D.D., Gurnett, D.A., 2010. Overlapping ionospheric and surface echoes observed by the Mars Express radar sounder near the Martian terminator. Geophys. Res. Lett. 37 doi:2010GL045859.

Duru, F., Gurnett, D.A., Morgan, D.D., Winningham, J.D., Frahm, R.A., Nagy, F., 2011. Nightside ionosphere of Mars studied with local electron densities: a general overview and electron density depressions. J. Geophys. Res. 116, A10316. http://dx.doi.org/10.1029/2011JA016835.

Edberg, N.J.T., Nilsson, H., Williams, A.O., Lester, M., Milan, S.E., Cowley, S.W.H., Fraenz, M., barabash, S., Futaana, Y., 2010. Pumping out the atmosphere of Mars through solar wind pressure pulses. Geophys. Res. Lett. 34, L09101. http://dx.doi.org/10.1029/2009GL041814.

Eparvier, F.G., Chamberlin, P.C., Woods, T.N., Thiemann, E.M.B., 2015. The solar Extreme ultraviolet monitor for MAVEN. Space Sci. Rev. http://dx.doi.org/10.1007/s11214-015-0195-2.

Espley, J.R., Cloutier, P.A., Crider, D.H., Brain, D.A., Acuna, M.H., 2005. Low-frequency plasma oscillations at Mars during the October 2003 solar storm. J. Geophys. Res. 110, A09S33.

Fraenz, M., Dubinin, E., Andrews, D., Barabash, S., Nilsson, H., Fedorov, A., 2015. Cold ion escape from Martian ionosphere. Planet. Space Sci. 119, 92–102.

Frahm, R.A., Sharber, J.R., Winningham, J.D., Wurz, P., Liemohn, M.W., Kallio, E., Yamauchi, M., Lundin, R., Barabash, S., Coates, A.J., Linder, D.R., Kozyra, J.U., Holmström, M., Jeffers, S.J., Andersson, H., McKenna-Lawler, S., 2006. Location of atmospheric photoelectron energy peaks within the Mars environment. Space Sci. Rev. 126, 389–402.

Fraenz, M., Dubinin, E., Nielsen, E., Woch, J., Barabash, S., Lundin, R., Fedorov, A., 2010. Transterminator ion flow in the Martian ionosphere. Planet. Space Sci. 58, 11. http://dx.doi.org/10.1016/j.pss.2010.06.009.

Forbes, T.G., et al., 2006. CME theory and models. Space Sci. Rev. 123, 251–302. http://dx.doi.org/10.1007/s11214-006-9019-8.

Futaana, Y., Barabash, S., Yamauchi, M., McKenna-Lawlor, S., Lundin, R., Luhmann, J.G., Brain, D., Carlsson, E., Sauvaud, J.–A., Winningham, J.D., Frahm, R.A., Wurz, P., Holstrom, M., Gunell, H., Kallio, E., Baumjohann, W., Lammer, H., Sharber, J.R., Hsieh, K.C., Andersson, H., Grigoriev, A., Brinkfeldt, K., Nilsson, H., Asamura, K., Zhang, T.L., Coates, A.J., Linder, D.R., Kataria, D.O., Curtis, C.C., Sandel, B.R., Fedorov, A., Mazelle, C., Thocaven, J.–J., Grande, M., Hannu, E., Koskinen, J., Sales, T., Schmidt, W., Riihela, P., Kozyra, J., Krupp, N., Woch, J., Fraenz, M., Dubinin, E., Orsini, S., Cerulli-Irelli, R., Mura, A., Milillo, A., Maggi, M., Roelof, E., Brandt, P., Szego, K., Scherrer, J., Bochsler, P., 2008. Mars Express and Venus Express multi-point observations of geoeffective solar flare events in December 2006. Planet. Space Sci. 56, 873–880.

Gopalswamy, N., Yashiro, S., Kaiser, M.L., Howard, R.A., Reames, D.V., Leske, R., Von Rosenvinge, T., 2002. Interacting coronal mass ejections and solar energetic particles. Astrophysical J. 572, L103–L107.

Gurnett, D.A., Kirchner, D.L., Huff, R.L., et al., 2005. Radar soundings of the ionosphere of Mars. Science 310, 1929–1933.

Gurnett, D.A., Morgan, D.D., Duru, F., Akalin, F., Winningham, J.D., Frahm, R.A., Dubinin, E., Barabash, S., 2010. Large density fluctuations in the Martian ionosphere as observed by the Mars Express radar sounder. ICARUS 206, 83–94.

Halekas, J.S., Taylor, E.R., Dalton, G., Johnson, G., Curtis, D.W., McFadden, J.P., Mitchell, D.L., Lin, R.P., Jakosky, B.M., 2015. The solar wind ion analyzer for MAVEN. Space Sci. Rev. 195, 125–151. http://dx.doi.org/10.1007/s11214-013-0029-z.

Halekas, J.S., Ruhunusiri, S., Harada, Y., Collinson, G., Mitchell, D.L., Mazelle, C., McFadden, J.P., Connerney, J.E.P., Espley, J.R., Eparvier, F., Luhmann, J.G., Jakosky, B.M., 2017. Structure, dynamics, and seasonal variability of the Mars-solar wind interaction: MAVEN Solar Wind Ion Analyzer in-flight performance and science results. J. Geophys. Res. Space Phys. 122, 547–578. http://dx.doi.org/10.1002/2016JA023167.

Howard, T., 2014. Space Weather and Coronal Mass Ejections. Springer-Verlag, New York.

Jakosky, et al., 2015. MAVEN observations of the response of Mars to an interplanetary coronal mass ejection. Science 350, 6261. http://dx.doi.org/10.1126/science.aad0210.

Larson, D.E., et al., 2015. The MAVEN solar energetic particle investigation. Space Sci. Rev. 195, 153–172. http://dx.doi.org/10.1007/s11214-015-0218-z.

Lillis, R.J., Fillingim, M.O., Peticolas, L.M., Brain, D.A., Lin, R.P., Bougher, S.W., 2009. Nightside ionosphere of Mars: modeling the effects of crustal magnetic fields and electron pitch angle distributions on electron impact ionization. J. Geophys. Res. 114, E11009. http://dx.doi.org/10.1029/2009JE003379.

Lundin, R., et al., 1989. First measurements of the ionospheric plasma escape from Mars. Nature 341, 609–612. http://dx.doi.org/10.1038/341609a0.

Lundin, R., Zakharov, A., Pellinen, R., Barabash, S.W., Borg, H., Dubinin, E.M., Hultqvist, B., Koskinen, H., Liede, I., Pissarenko, N., 1990. ASPERA/PHOBOS measurements of the ion outflow from the martian ionosphere. Geophy. Res. Lett. 17 (6), 873–876.

Lundin, R., Barabash, S., Holmstrom, M., Nilsson, H., Yamauchi, M., Fraenz, M., Dubinin, E.M., 2008. A comet-like escape of ionospheric plasma from Mars. Geophys. Res. Lett. 35, L18203. http://dx.doi.org/10.1029/2008GL034811.

Lundin, R., Barabash, S., Holmstrom, M., Nilsson, H., Futaana, Y., Ramstad, R., Yamauchi, M., Dubinin, E., Fraenz, M., 2013. Solar cycle effects on the ion escape from Mars. Geophys. Res. Let. 40, 6028–6032. http://dx.doi.org/10.1002/2013GL058154.

Ma, Y., Nagy, A.F., 2007. Ion escape fluxes from Mars. Geophys. Res. Lett. 34, L08201. http://dx.doi.org/10.1029/2006GL029208.

Ma, Y., Fang, X., Russell, C.T., Nagy, A.F., Toth, G., Luhmann, J.G., Brain, D.A., Dong, C., 2014. Effects of crustal field rotation on the solar wind plasma interaction with Mars. Geophys. Res. Let. 41, 6563–6569. http://dx.doi.org/10.1002/2014GL060785.

McFadden, J.P., Livi, R., Luhmann, J., Connerney, J., Mitchell, D., Mazelle, C., Andersson, L., Jakosky, B., 2015. Structure of the Martian ionosphere and atmospheric loss: MAVEN STATIC first results. Lunar Planet. Sci. Conf. abstract 2899.

McKenna-Lawlor, S.M.P., et al., 2008. Predicting interplanetary shock arrivals at Earth, Mars, and Venus: a real-time modeling experiment following the solar flares of 5–14 December 2006. J. Geophys. Res. 113 (A6) http://dx.doi.org/10.1029/2007JA012577.

Morgan, D.D., Gurnett, D.A., Kirchner, D.L., Huff, R.L., Brain, D.A., Boynton, W.V., Acuna, M.H., Plaut, J.J., Picardi, G., 2006. Solar control of radar wave absorption by the Martian ionosphere. Geophys. Res. Let. 33, L13202. http://dx.doi.org/10.1029/2006GL026637.

Morgan, D.D., Dieval, C., Gurnett, D.A., Duru, F., Dubinin, E.M., Fraenz, M., Andrews, D.J., Opgenoorth, H.J., Ulusen, D., Mitrofanov, I., Plaut, J.J., 2014. Effects of a strong ICME on the martian ionosphere as detected by Mars express and Mars Odyssey. J. Geophys. Res. 119, 5891–5908. http://dx.doi.org/10.1002/2013JA019522.

Nemec, F., Morgan, D.D., Dieval, C., Gurnett, D.A., Futaana, Y., 2014. Enhanced ionization of the Martian nightside ionosphere during solar energetic particle events. Geophys. Res. Lett. 41, 793–798. http://dx.doi.org/10.1002/2013GL058895.

Nemec, F., Morgan, D.D., Dieval, C., Gurnett, D.A., 2015. Intensity of nightside MARSIS AIS surface reflections and implications for low-altitude ionospheric densities. J. Geophys. Res. 120 http://dx.doi.org/10.1002/2014JA020888.

Nilsson, H., Edberg, N.J.T., Stenberg, G., Barabash, S., Holmstrom, M., Futaana, Y., Lundin, R., Fedorov, A., 2011. Heavy ion escape from Mars, influence from solar wind conditions and crustal magnetic fields. Icarus 215 (2), 475–484.

Opgenoorth, H. J., Andrews, D. J., Fraenz, M., Lester, M., Edberg, N. J. T., Morgan, D., Duru, F., Witasse, O., Williams, A. O., 2013. Mars ionospheric response to solar wind variability. J. Geophys. Res. Space Phys. 118, 6558–6587. http://dx.doi.org/10.1002/jgra.50537.

Picardi, G., Biccari, D., Seu, R., et al., 2004. MARSIS: Mars advanced radar for subsurface and ionosphere sounding. In: Wilson, A. (Ed.), Mars Express: a European Mission to Red Planet, SP-1240. European Space Agency Publication Division, Noordwijk, Netherlands, pp. 51–70.

Ramstad, R., Futaana, Y., Barabash, S., Nilsson, H., del Campo, S.M., Lundin, B.R., Schwingenschuh, K., 2013. Phobos 2/ASPERA data revisited: planetary ion escape rate from Mars near 1989 solar maximum. Geophys. Res. Lett. 40, 477–481. http://dx.doi.org/10.1002/grl.50149.

Reames, D.V., 1999. Particle acceleration at the Sun and in the heliosphere. Space Sci. Rev. 90, 413–491.

Vignes, D., Mazelle, C., Rme, H., Acuna, M.H., Connerney, J.E.P., Lin, R.P., Mitchell, D.L., Cloutier, P., Crider, D.H., Ness, N.F., 2000. The solar wind interaction with Mars: location and shapes of the bow shock and the magnetic pile-up boundary from the observations of the MAG/ER experiment onboard Mars. Geophys. Res. Lett. 27 (1), 49–52.

Withers, P., Fillingim, M.O., Lillis, R.J., Häusler, B., Hinson, D.P., Tyler, G.L., Pätzold, M., Peter, K., Tellmann, S., Witasse, O., 2012. Observations of the nightside ionosphere of Mars by the Mars express radio science experiment (MaRS). J. Geophys. Res. 117, A12307. http://dx.doi.org/10.1029/2012JA018185.